iScience

CellPress
OPEN ACCESS

Article

Mathematical multi-compartment modeling of chronic lymphocytic leukemia cell kinetics under ibrutinib

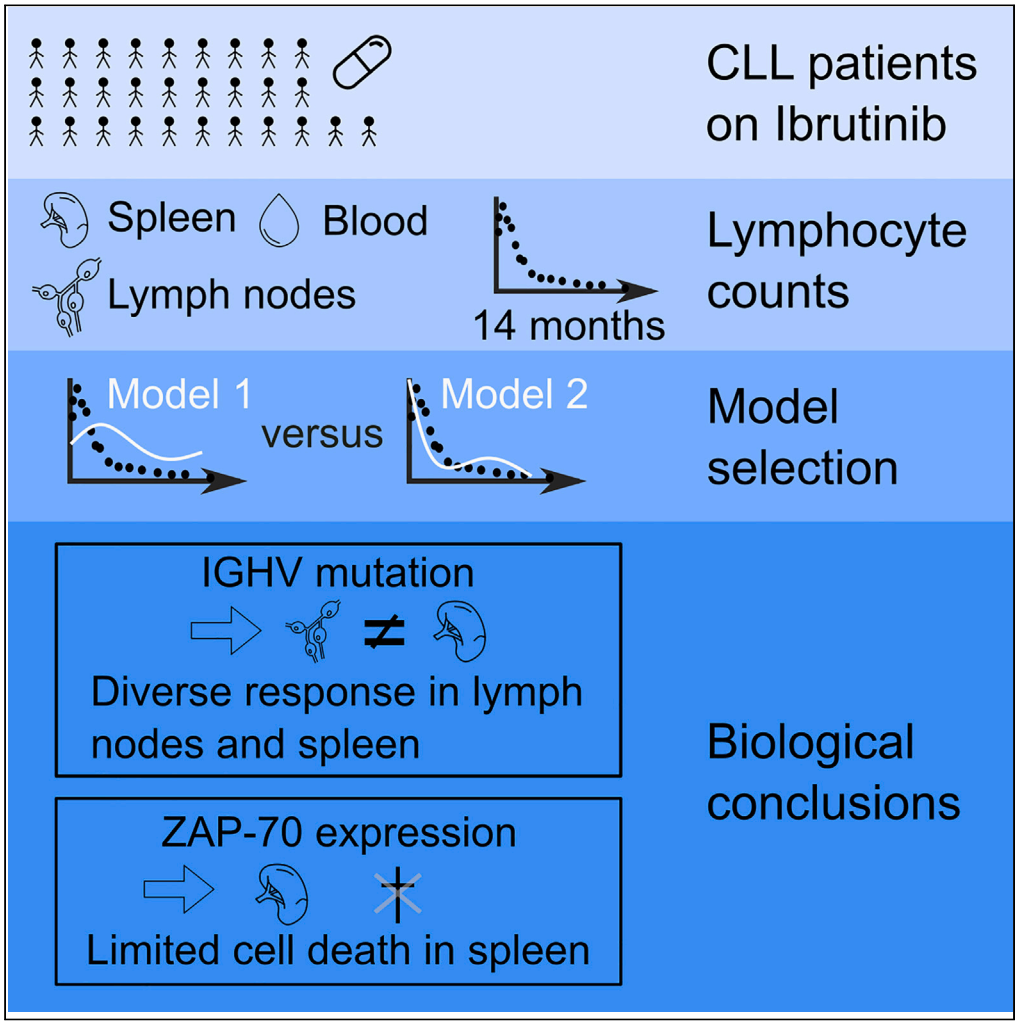

Melanie Schulz, Sanne Bleser, Manouk Groels, Dragan Bošnački, Jan A. Burger, Nicholas Chiorazzi, Carsten Marr

carsten.marr@helmholtz-munich.de

Highlights

Introducing constant subcompartments improves a published model for CLL kinetics

Diverse response to Ibrutinib in lymph nodes/spleen for patients without IGHV mutation

ZAP-70 expression is linked to less cell death in the spleen

Schulz et al., iScience 27, 111242
December 20, 2024
https://doi.org/10.1016/j.isci.2024.111242

iScience

CellPress
OPEN ACCESS

Article

Mathematical multi-compartment modeling of chronic lymphocytic leukemia cell kinetics under ibrutinib

Melanie Schulz,[1,2] Sanne Bleser,[1,3] Manouk Groels,[1,3] Dragan Bošnački,[3] Jan A. Burger,[4] Nicholas Chiorazzi,[5,6] and Carsten Marr[1,7,*]

SUMMARY

The Bruton tyrosine kinase inhibitor ibrutinib is an effective treatment for patients with chronic lymphocytic leukemia (CLL). While it rapidly reduces lymph node and spleen size, it initially increases the number of lymphocytes in the blood due to cell redistribution. A previously published mathematical model described and quantified those cell kinetics. Here, we propose an alternative mechanistic model that outperforms the previous model in 26 of 29 patients. Our model introduces constant subcompartments for healthy lymphocytes and benign tissue and treats spleen and lymph nodes as separate compartments. This three-compartment model (comprising blood, spleen, and lymph nodes) performed significantly better in patients without a mutation in the IGHV gene, indicating a diverse response to ibrutinib for cells residing in lymph nodes and spleen. Additionally, high ZAP-70 expression was linked to less cell death in the spleen. Overall, our study enhances understanding of CLL genetics and patient response to ibrutinib and provides a framework applicable to the study of similar drugs.

INTRODUCTION

In Chronic Lymphocytic Leukemia (CLL), the most common leukemia in Western countries, immature B-lymphocytes proliferate and accumulate within lymph nodes, spleen, bone marrow and peripheral blood.[1,2] Intercellular signaling has been shown to be critical in the pathogenesis and progression of the disease. It can be targeted by drugs such as ibrutinib, which inhibits Brutin tyrosine kinase, an essential kinase in B cell receptor signaling and activation.[3,4] During the early stage of therapy with ibrutinib, an increased number of lymphocytes within the peripheral blood has been observed in many patients when applied in clinical practice.[2] It has been suggested that this is not due to disease progression but due to a compartment shift where cells redistribute from lymph nodes and spleen to the circulating blood.[2]

To describe and quantify this effect, a mathematical model of lymphocyte kinetics (derived from a previous model[5]) has been applied to a cohort of 10 patients with CLL under treatment with ibrutinib.[6] The model consists of two compartments represented by two kinetic observables: (i) The total number of CLL cells within the lymph tissue, comprising both spleen and lymph nodes (n_{lt}), (ii) The total number of CLL cells within the peripheral blood (n_{pb}). It allows for cell death in both compartments and a redistribution from lymph tissue to blood. To avoid total clearing of lymphocytes in the limit of infinite time ($\lim_{t\to\infty}(n_{\mathrm{lt}}(t)+n_{\mathrm{pb}}(t)) = 0$), a constant influx into the lymph tissue has been added to the model. Analysis of the modeling results showed that the decrease in tissue volume could not be explained by a compartment shift alone but that CLL cells directly died in the lymph tissue.[6] Furthermore, the authors showed that ibrutinib increased the death rate of CLL cells within blood and tissue by a factor 3 and 5, respectively. The approach was adopted in a later study where the same mathematical model was applied to a cohort of 29 patients and the estimated parameters quantifying cell death in the lymph tissue as well as differences between several patient groups have been analyzed.[7]

In this study, we suggest two simplifications to the previously published model and compare their fit to clinical data. First, we investigate long-term stabilization that allows for direct biological interpretation and test if all kinetic reactions in the mathematical model are needed to describe the data. Second, we evaluate if the model can be improved by treating spleen and lymph nodes, measured separately via computed tomography (CT) scans, as distinct compartments. We compare the performance of our approach to the existing model on the dataset used in earlier studies.[7] The model used therein is referred to as the reference model in the following.

[1]Institute of AI for Health, Helmholtz Munich – German Research Centre for Environmental Health, Neuherberg, Germany
[2]TUM School of Mathematics, Technical University of Munich, Munich, Germany
[3]Faculty of Biomedical Engineering, Technichal University Eindhoven, Eindhoven, the Netherlands
[4]Department of Leukemia, Division of Cancer Medicine, The University of Texas MD Anderson Cancer Center, Houston, TX, USA
[5]Feinstein Institutes for Medical Research, Northwell Health, Manhasset, NY 11030, USA
[6]Zucker School of Medicine at Hofstra/Northwell, Hempstead, NY 11549, USA
[7]Lead contact
*Correspondence: carsten.marr@helmholtz-munich.de
https://doi.org/10.1016/j.isci.2024.111242

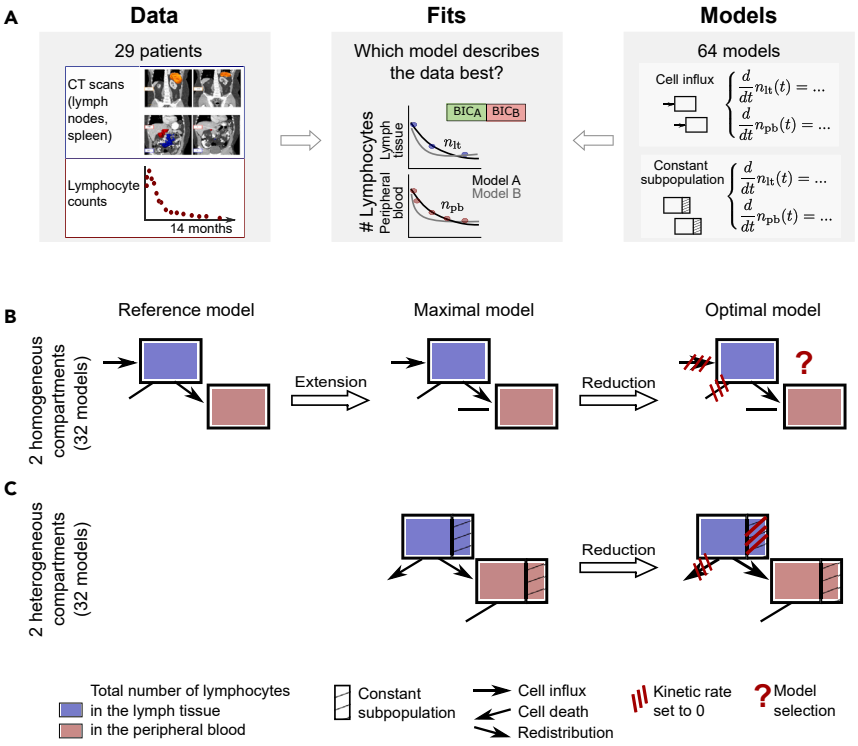

Figure 1. Mathematical 2-compartment models describing the lymphocyte counts in a patient's lymph tissue and peripheral blood during the treatment of CLL with ibrutinib can be split up into two families and reduced by fitting to measured data

(A) The cohort of 29 patients was monitored over a time course of up to 14 months after the start of treatment with ibrutinib. Volumetric estimations of lymph nodes and spleen obtained from CT scans and repeated measurements of lymphocyte counts in the peripheral blood were used to fit and compare 64 mathematical models containing either influx or constant subpopulations for each of the 29 patients.

(B) The reference model belongs to the homogeneous model family comprising models where all cells in a compartment, namely lymph tissue (blue) and peripheral blood (red), are assumed to show the same reaction to ibrutinib. Stabilization of the system in the limit of infinite time is obtained by adding a constant influx to one or both compartments. In the maximal model of each family, all 5 possible kinetic rates are present. To analyze if all suggested cell fluxes are relevant, we compared a total of 32 models within the homogeneous family by setting one or more parameters to 0 to find the optimal homogeneous 2-compartment model that best fits the longitudinal clinical data. The model comprising all five reactions is denoted as the *maximal* model of the family, whereas, for each patient, we refer to the *optimal* model as the best performing one as selected by the BIC. Note that, as model selection was performed for every patient individually, the architecture of the optimal model might differ between patients.

(C) Within the family of heterogeneous models, constant influxes are replaced by constant subpopulations representing cells that are not affected by ibrutinib. Model reduction removed unnecessary parameters and resulted in the optimal heterogeneous 2-compartment model.

Clinical data

The data used in our study comprises information on 29 patients with CLL treated with ibrutinib. It has been courteously provided by Jan Burger and was used in their study.[7] For every patient, basic information such as gender, weight and disease progression have been recorded at therapy start. During treatment, 12 to 32 measurements of lymphocyte counts per microliter blood and 2 to 3 CT based volumetric estimations of lymph nodes and spleen to observe the cancer burden within peripheral blood and lymph tissue, respectively, have been collected over a time course of up to 14 months.[7] See Figure 1A for an overview and Section clinical data in the supplemental material for details on the data.

RESULTS

Models with two homogeneous or heterogeneous compartments

To model lymphocyte kinetics under treatment with ibrutinib with two compartments, we compared a total of 64 models grouped into two model families, differing in their way of obtaining long-term stabilization, i.e., constant influx or subcompartments. The considered models predict the total number of lymphocytes within the peripheral blood and the lymph tissue at any timepoint during therapy. For every patient, all models have been fitted to total lymphocyte counts estimated from the measurement data to select the best performing model based on the Bayesian Information Criterion (BIC). The overall approach is visualized in Figure 1A.

Details on the preprocessing and fitting procedure can be found in the methods section.

Starting with the reference model (Figure 1B) we investigated if adding a constant influx to the peripheral blood compartment or reduction of the kinetic reactions would lead to improvements. Specifically, we considered five kinetic reactions that can be either included or

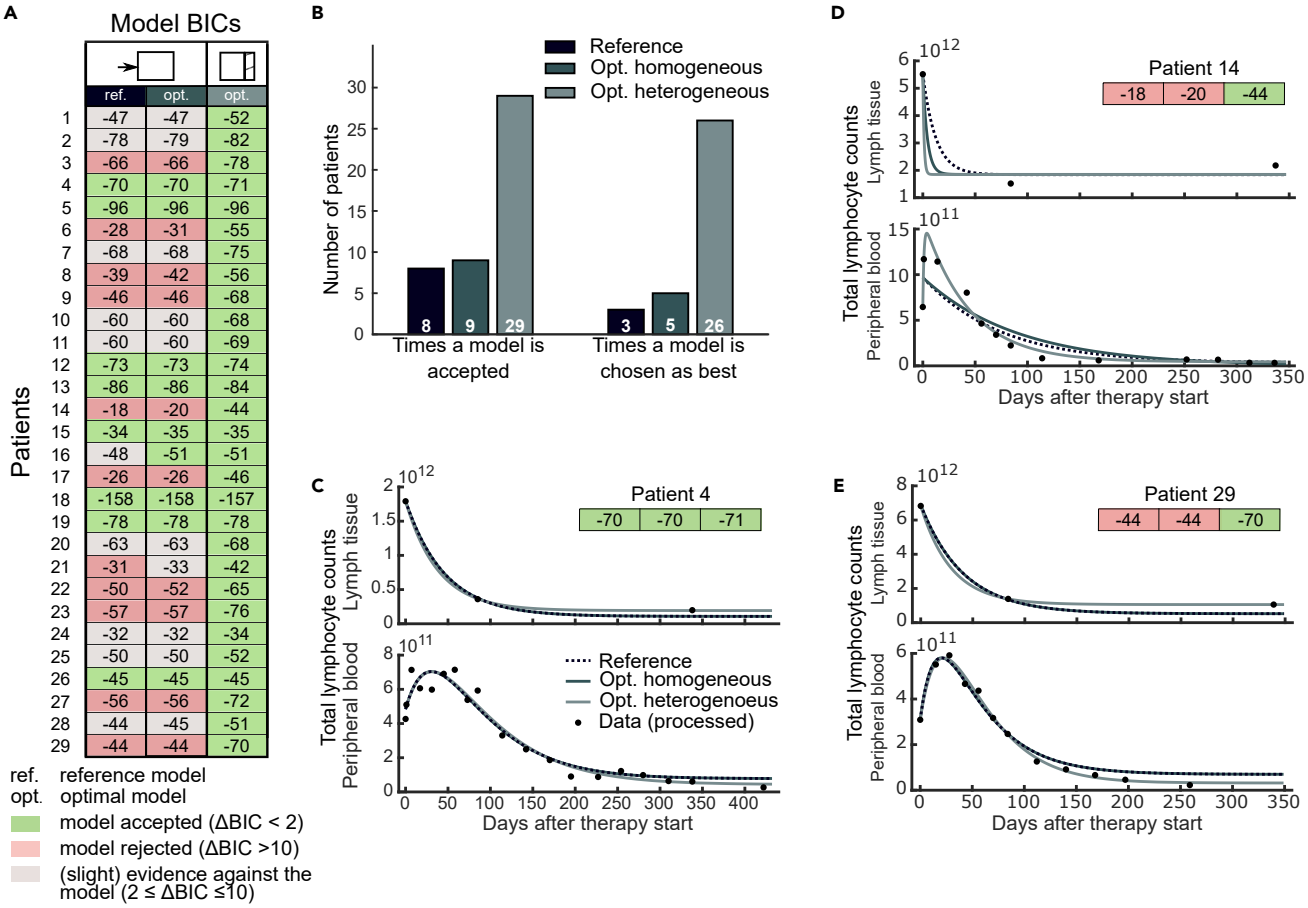

Figure 2. Heterogeneous 2-compartment models describe lymphocyte kinetics under ibrutinib treatment better than homogeneous models

(A) BIC values for 64 2-compartment models. Model selection based on minimal BIC identified the minimal heterogeneous model as the most suitable to describe lymphocyte kinetics under therapy with ibrutinib. We present the BIC scores for the reference model, the optimal homogeneous model, and the optimal heterogeneous model. The numerical values represent the computed BIC scores for each model and patient, visually differentiated and assessed based on their BIC difference in comparison to the best-performing model on a patient-wise basis. As model reduction was performed for each patient individually, the optimal models do not necessarily include the same kinetic reactions for all patients.

(B) The optimal heterogeneous 2-compartment model was accepted for all 29 patients and was thus able to sufficiently describe all the data. It fitted measured lymphocyte counts best in 26 out of the 29 patients and thus outperformed the previously considered model as well as the models within the corresponding homogeneous model family.

(C–E) Exemplary model fits for patients with both homogeneous and heterogeneous models performing comparably (C) or the optimal heterogeneous model outperforming the remaining ones, once mainly in the earlier (D), once in the later (E) observation phase.

excluded, namely cell death in the lymph tissue (i) and blood (ii) compartment, influx into lymph (iii) and blood (iv) compartment, as well as distribution from lymph tissue to peripheral blood compartment (v). Combining all possibilities of a reaction being considered or not considered yields a total of $2^5 = 32$ models. We call them the *homogeneous* model family as they assume that all lymphocytes react to ibrutinib in the same way. Alternatively, we suggest to regard the compartments as heterogeneous entities, comprising cells that either respond or do not respond to ibrutinib (Figure 1C). In the lymph nodes and spleen, this non-responding subpopulation of constant size might represent tissue not consisting of lymphocytes, in the peripheral blood, it can refer to cells not affected by ibrutinib.[8] Models with constant subpopulations instead of constant influxes are called *heterogeneous* models in the following. Again, we investigated if the kinetic reactions of cell death in both lymph tissue and peripheral blood as well as the redistribution and constant subcompartments are needed to explain the data by BIC (Figures 1B and 1C). The corresponding mathematical equations and solutions are derived in the methods section.

Quantitative comparison of 2-compartment models

We performed patient-wise model selection based on the Bayesian Information Criterion (BIC) to find and compare the best models of each model family. For every patient, the model with the lowest BIC was considered the optimal model. We accepted models in case their BIC differed

from the best BIC by less than 2, whereas we rejected models when the respective BIC values differed by more than 10 (Figure 2). Fitted to 29 patients, the reference model and the optimal homogeneous model were accepted for only 8 and 9 patients, respectively (Figures 2A and 2B). In contrast, the optimal heterogeneous model was accepted for all patients and was thus the only one sufficient to explain all measurement data. Furthermore, it was selected as best for 26 patients, while only in 5 patients the optimal homogeneous model was picked (Figure 2B). For 3 out of those 5 patients, the reference model was equal to the optimal homogeneous model, and both models were rated as best. For patients 25 and 16, the performance of the optimal homogeneous and heterogeneous models coincided, and both models were classified as best. Exemplary fits of the optimal homogeneous and heterogeneous model demonstrate that while the models yield comparable results for some patients (patient 4, Figure 2C), the optimal heterogeneous model provides superior explanations for the data across both early and late therapy stages in other patients (patient 14, Figure 2D, and patient 29, Figure 2E).

Models with three heterogeneous compartments

In all models considered so far, we followed previous assumptions that lymphocytes within the spleen and lymph nodes behave equally, and therefore both tissue sites can be treated as one compartment.[5–7] However, this hypothesis has been challenged, and a compartment shift from lymph nodes to spleen has been described.[9] Another study quantifying tumor burden in blood, lymph nodes, spleen, and bone marrow separately at several timepoints during therapy with ibrutinib stated that the initial rise in lymphocytosis was mainly due to the release of cells from the lymph nodes, also indicating distinct behavior of cells residing in lymph nodes and spleen.[10] Therefore, we extended the model to three compartments and compared model performance on our dataset. As the heterogeneous model family had outperformed the set of homogeneous models on two compartments, we did not consider homogeneous models for the model extension. To determine the set of models considered, we assumed that cells can, but do not have to, migrate between lymph nodes and peripheral blood and between spleen and peripheral blood. Between the two respective compartments, we allowed redistributions in both directions simultaneously. Since lymphocytes can only reach the spleen directly from peripheral blood or exit into peripheral blood,[11] we did not consider pathways between the spleen and lymph node. Cell death and constant subpopulations may or may not be present in all compartments. In this way, we obtained a set of 1024 potential models. As the 3-compartment models are able to describe diverse behavior of cells within the spleen and lymph nodes, we omitted the adaption of the spleen volume as described in Section models with two homogeneous or heterogeneous compartments. To reduce computational time, we performed a hierarchical model selection approach: We partitioned models into 16 clusters based on the existence and direction of redistribution processes. For each model cluster, we first optimized the maximal model, i.e., the model where cell death and constant subcompartments are apparent in all considered tissues. Second, we applied the BIC with a threshold of 10 to select the maximal models that were not rejected and optimized the submodels of the corresponding model set (Figure 3A). The best performing model with respect to the BIC is denoted as the optimal 3-compartment model. The approach was performed for every patient individually.

Quantitative comparison of 2- and 3-compartment models

Whereas the 2-compartment models were fitted to combined lymph tissue data after the adaption of the spleen volume (Section models with two homogeneous or heterogeneous compartments), the 3-compartment model was fitted to lymphocyte counts estimated from spleen and lymph node volumes separately, and without further adaptions. To compare model performance quantitatively via BIC, the solutions must be projected to predict the same target data. We used the total number of lymphocytes estimated from blood counts and the raw lymph tissue data (comprising both lymph nodes and spleen). To predict those measurements from the 3-compartment model, the solutions of the spleen and lymph node compartments need to be summed up. For the 2-compartment model, the volumetric adaptions (Section models with two homogeneous or heterogeneous compartments) need to be reverted as described in the methods section. In Figure 3B, we show the BIC values of the selected models for every patient computed on the lymphocytes estimated from peripheral blood and raw tissue volume. The optimal heterogeneous model with two compartments was accepted for 26 patients, while the 3-compartment model was accepted for 9 patients (Figure 3C). Remarkably, there are three patients (patients 1, 23, and 25) where all 2-compartment models have been rejected, indicating that a model with three compartments is necessary to explain the observed data. In Figures 3D–3F we show the fits to the reference model, the best 2-compartment model, and the 3-compartment model for those patients, all adapted to predict the raw tissue data. Notably, all three patients have no mutation in the IGHV gene, which is known to be related to a less favorable prognosis. We thus investigate a correlation between mutational status and 3-compartment model performance. The analysis is performed on only 27 patients as two patients (patients 8 and 26) have unknown mutational status. Indeed, we find that the IGHV mutational status significantly correlates with the qualitative performance of the 3-compartment model with a p-value of 0.0145 (Chi-Squared test, see Table 1). A one-sided Wilcoxon Rank-sum test supports the observation that the 3-compartment models perform better on patients with unmutated CLL than on the remaining cohort ($p = 0.0041$).

Clinical analysis

To gain more insights into different lymphocyte kinetics within lymph nodes and spleen, we analyzed the parameters of the best 3-compartment model for each patient (see Figure 4). To obtain maximally reliable results, we removed 13 patients where one or more parameters of the best model were not identifiable or for whom the best 3-compartment model was rejected (BIC difference more than 10) as compared to the 2-compartment model (death rates in spleen and lymph nodes are identical in the 2-compartment model). Following this

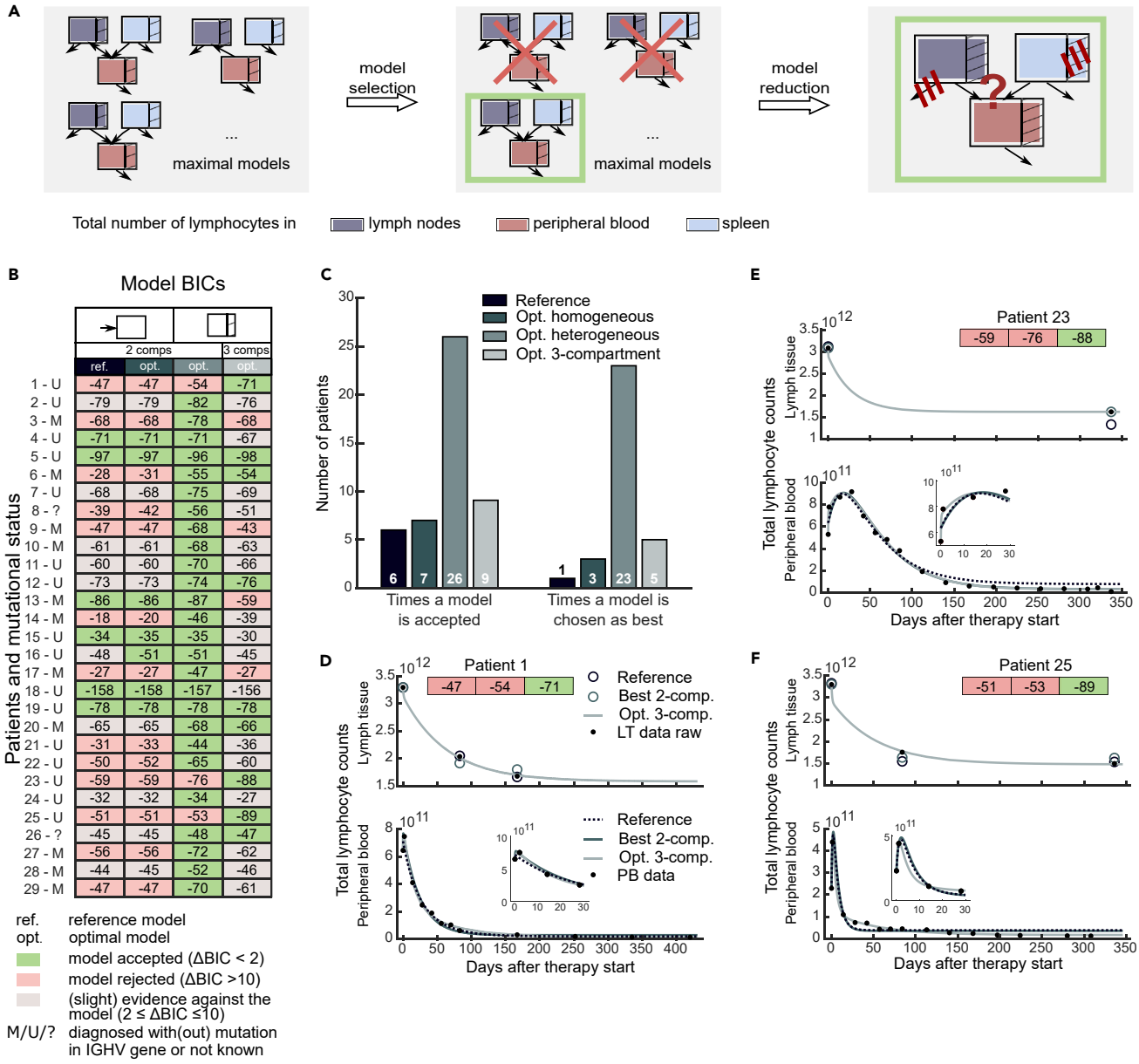

Figure 3. Only for three patients, a 3-compartment model explained the data significantly better than any 2-compartment model

(A) Hierarchical model selection process. All 1024 models were grouped based on the existence and direction of redistribution processes. First, parameters of the most complex models of each model cluster were optimized and, based on BIC, the best performing complex models were selected. Second, the selected complex models were reduced by setting one or more parameters to 0. Again, BIC was applied to the resulting set of models to find the best 3-compartment model. The model selection pipeline was applied to every patient individually.

(B) For three patients, all without a mutation in the IGHV gene, the 3-compartment model was the only one accepted, indicating the diverse behavior of cells within the spleen and the lymph nodes.

(C) The 3-compartment model was accepted for 9 out of 29 patients and selected as best for 5 patients. If two model performances coincided, both were rated as best.

(D–F) Comparison of fits obtained with 2-and 3-compartment models, respectively, for patients 1 (D), 23 (E), and 25 (F), where all 2-compartment models have been rejected. For all three patients, the 3-compartment model shows superior performance in both the lymph tissue and the peripheral blood prediction.

approach, we see that decline rates (defined as the sum of death and redistribution rate, quantifying all cells leaving the compartment) are significantly higher in the lymph nodes than in the spleen ($p = 0.017$, Paired samples Wilcoxon Rank-sum test, see Figure 4A). We could not find if that was caused by higher redistribution or death rates (see Figures 4B and 4C). Note that the occurrence of cell death in lymph nodes or spleen is predicted for only 9 of the 16 patients.

Table 1. Performance of the 3-compartment model among patients with and without mutation in the IGHV gene

	Patients with unmutated CLL	Patients with mutated CLL
3-compartment model accepted	7	1
(Slight) evidence against 3-compartment model	9	6
3-compartment model rejected	0	4
Total	16	11

Furthermore, we analyzed correlations of the kinetic parameter values with clinical parameters such as IGHV mutational status or level of ZAP-70 expression (see Figure 4D). We do not find significant differences in rates between patients with mutated and unmutated CLL. However, our analysis suggests that cell death in the spleen occurs significantly less for ZAP-70 positive patients ($p = 0.0048$, one-sided Wilcoxon Rank-sum test. This is in line with previous findings suggesting that ZAP-70 promotes cell survival and microenvironment interactions.[12]

DISCUSSION

While ibrutinib achieved promising results in clinical studies, the underlying kinetics are yet not fully understood.[4] To gain insights into the mechanisms of cell redistribution and cell death during treatment with ibrutinib, a mechanistic 2-compartment model that contains a constant influx into the lymph tissue compartment has been applied before.[6] This influx helped to stabilize model performance for infinite times but lacked a physiological interpretation. Our results propose that obtaining longterm stabilization by using constant subcompartments is more suitable than adding a constant influx as revealed by model comparison based on the BIC. Furthermore, constant subcompartments allow for a direct biological interpretation, namely healthy tissue or non cancerous B-cells or other types of lymphocytes not responding to the ibrutinib therapy. Whereas the 2-compartment models combine lymph nodes and spleen into one observable, we further investigated models where both tissues are treated as separate compartments. A model with an added third compartment was accepted in 9 out of 29 patients and significantly improved fitting for 3 patients. The results might be influenced by our approach of model comparison that was defensive with respect to the 3-compartment model due to several reasons: (i) In our objective function adopted from previous studies,[6,7] all included model compartments are weighted equally. The same holds true for the objective function used for comparing the 2- to the 3-compartment models. Thus, while the 2-compartment models have been tuned to optimally perform on the lymph tissue and peripheral blood compartments weighted equally, the 3-compartment models were optimized to provide the best results when weighing blood, spleen, and lymph nodes with 1/3 each. Using an objective function that gives peripheral blood a weight of 1/2 when fitting the 3-compartment data might improve the competitiveness of the 3-compartment models. Furthermore, it might prevent overfitting the lymph tissue data. (ii) Another aspect favoring 2- over 3-compartment models is the applied criterion for model selection, the BIC, as it punishes more complex models. With the 3-compartment models having more separate entities and thus, in general, more kinetic reactions and parameters, 2-compartment models have been selected in cases where they describe the measurement data equally well as 3-compartment models. On the other hand, the 3-compartment model has several advantages, even if it was accepted for only 9 patients. First, it is the only one giving insights into the diverse kinetics of cells within lymph nodes and spleen. Second, while with the 2-compartment model, we can only predict lymph tissue volume at the dates measurements were taken, as it only models the adapted data which is supposed to represent the cancerous tissue, the 3-compartment model predicts the tissue volume over the whole time course. Finally, whereas a biological prior has been applied in former studies[6,7] when adapting the volumetric estimations before the parameter optimization, the 3-compartment model is able to describe and predict different kinetics within the lymph nodes and spleen. It thus allows to fit to lymphocytes estimated from the raw measurement data, providing a more data-driven approach.

An increased spleen size during the first weeks of therapy caused by a compartment shift from lymph nodes to the spleen via the blood compartment has been suggested.[9] We find cellular redistribution from the peripheral blood toward the spleen for only two patients. An increased spleen volume is not predicted for any of the patients based on the best performing 3-compartment model. Notably, while the mentioned study included only three patients,[9] our investigation comprised a cohort of 29 patients. The heterogeneity of the disease and patients' reactions to ibrutinib might be the reason for the contradicting results. Furthermore, the second tissue measurement available in our study was taken after around 80 days, whereas in Mayerhoefer et al.,[9] follow up CT scans have been conducted at time points very early in therapy, namely after one, two, or three weeks. We cannot rule out that our results would differ having volumetric estimations in the early therapy stage available, providing more detailed insights into the immediate kinetic response to the treatment.

While the analysis of death rates in the lymph tissue played an essential role in Wodarz et al.[6] and Burger et al.,[7] our results favor models with no cell death in the lymph tissue in 16 out of 29 patients. For those, we predict the lymphoid organs to function mainly as transition compartments while cell death takes place in the peripheral blood. Model selection suggested that the immediate decrease of lymph tissue volume can be explained by redistribution only for a majority of the cohort, contradicting the results in Wodarz et al.[6] However, even if a model without cell death in lymphoid organs might be preferred by the BIC, we cannot exclude that cell death takes place. The model selection results rather suggest that models without cell death in lymph tissue are sufficient to describe the clinical data, predicting that redistribution plays a major role in the reduction of the lymph tissue volume.

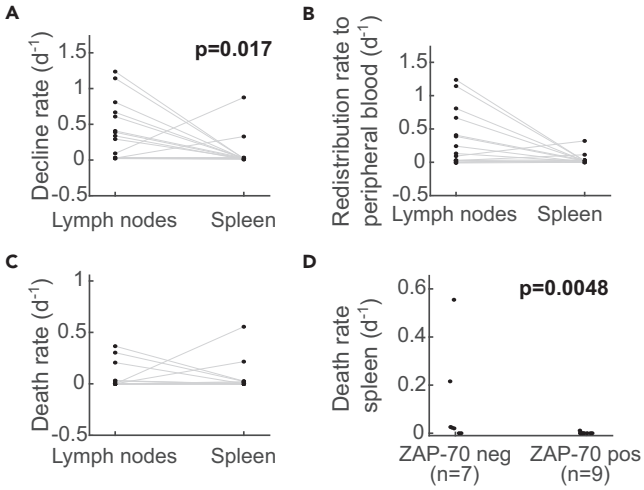

Figure 4. Optimized rates of the 3-compartment model suggest a significantly faster decline of lymphocytes within lymph nodes than in the spleen and significantly less cell death for patients with ZAP-70 expression

(A) Decline rates, defined as the sum of death and redistribution rates, are significantly higher in the lymph nodes than in the spleen ($p = 0.017$, paired Wilcoxon Rank-sum Test). Gray lines connect the respective kinetic rates (black dots) of a patient.

(B) Redistribution rates from lymph nodes to peripheral blood.

(C) We do not find significant differences in death rates of cells residing in lymph nodes or spleen, respectively. Cell death in lymph nodes is predicted for 5 patients, and cell death in the spleen for 6 patients. For 7 patients, no cell death in lymph nodes or spleen is suggested.

(D) Cell death in the spleen occurs significantly less for ZAP-70 negative patients compared to patients expressing ZAP-70 ($p = 0.0048$, one-sided, unpaired Wilcoxon Rank-sum Test). Most ZAP-70 negative patients (5 out of 7) are expected to show this cell death in the spleen, while only one ZAP-70 positive patient (1 out of 9) is predicted to exhibit it.

In a former study, the death rate of cells in the lymph tissue has been related to patients' mutational status in the IGHV gene and unmutated CLL has been found to be correlated with higher death rates.[7] Although we did not observe significant differences in the death rates when comparing patients with mutated and unmutated CLL, an interesting pattern emerged when evaluating the performance of the 3-compartment models compared to the 2-compartment models. Specifically, we found that the 3-compartment models exhibited significantly better performance in patients with unmutated CLL compared to those with mutated CLL. This observation suggests a potentially more diverse response of cells within the spleen and lymph nodes among patients with unmutated CLL.

Additionally, our analysis revealed a noteworthy association between cell death in the spleen and ZAP-70 expression level. Specifically, we observed a significant reduction in cell death in the spleen among patients with high ZAP-70 expression compared to the remaining patients, underscoring the potential influence of this molecular characteristic on disease progression and treatment response. As this analysis was performed on the subset of patients, for whom the 3-compartment model was accepted and all parameters could be reliably estimated ($n = 16$), the significance of the result is limited by a small sample size, and further research must be done to investigate our observation.

As bone marrow is an essential player in human hematopoiesis, the effect of ibrutinib on the accumulation of CLL cells there might provide additional insights. In Rooij et al.,[8] a clearance of cancer cells from the bone marrow was suggested, comparable to the clearing of the lymph tissue. An extension of the mathematical model to include the bone marrow as the third or fourth compartment might improve the understanding of a patient's reaction to ibrutinib, but is left to further experimental and computational studies.

Limitations of the study

Our study provides a computational framework to model CLL cell kinetics under Ibrutinib. While we suggest mathematical models that describe the experimental data better than a model introduced in previous research, we cannot identify one model or model family that performs best on all patients. This might be due to the heterogeneity of the disease or due to the limited amount of data in all tissues but the peripheral blood. With a larger sample size and more measurements available, statistically more significant conclusions about the relation of preferred models, kinetic parameters, and disease sub-types might be drawn.

RESOURCE AVAILABILITY

Lead contact

Further information and requests should be directed to and will be fulfilled by the Lead Contact Carsten Marr (carsten.marr@helmholtz-munich.de).

Materials availability

This study did not generate new materials.

Data and code availability

- Anonymized patient data reported in this article will be shared by the lead contact upon request.
- All computational experiments were implemented and performed with the MATLAB version of R2017b. Code of ODE model simulation and parameter optimization can be found in zenodo, link is listed in the key resources table.
- Any additional information required to reanalyze the data reported in this article is available from the lead contact upon request.

ACKNOWLEDGMENTS

We thank Ivan Kukuljan, Nora Emmermann, and Dominik Waibel (Munich) for critical reading and helpful comments, and Maartje Hoogeveen for preliminary work on the reference model.

Carsten Marr acknowledges funding from the European Research Council (ERC), grant agreement no. 866411, and financial support from the Hightech Agenda Bayern.

AUTHOR CONTRIBUTIONS

M.S. and C.M. wrote the article with feedback from all authors. M.S., S.B., and M.G. implemented the MATLAB code of the models, fitted the data, and checked the computational accuracy with C.M. and D.B. J.B. and N.C. provided the patient data and the biological prior knowledge. C.M. and D.B. supervised the work. All authors discussed the results and approved the article.

DECLARATION OF INTERESTS

The authors declare no competing interests.

STAR★METHODS

Detailed methods are provided in the online version of this paper and include the following:

- KEY RESOURCES TABLE
- METHOD DETAILS
  - Clinical data
  - Data preprocessing
  - Model design
  - Differential equations
  - Parameter optimization
  - Model selection
- QUANTIFICATION AND STATISTICAL ANALYSIS

SUPPLEMENTAL INFORMATION

Supplemental information can be found online at https://doi.org/10.1016/j.isci.2024.111242.

Received: December 19, 2023
Revised: July 17, 2024
Accepted: October 22, 2024
Published: October 28, 2024

REFERENCES

1. Ponader, S., Chen, S.S., Buggy, J.J., Balakrishnan, K., Gandhi, V., Wierda, W.G., Keating, M.J., O'Brien, S., Chiorazzi, N., and Burger, J.A. (2012). The Bruton tyrosine kinase inhibitor PCI-32765 thwarts chronic lymphocytic leukemia cell survival and tissue homing in vitro and in vivo. Blood *119*, 1182–1189.
2. de Rooij, M.F.M., Kuil, A., Geest, C.R., Eldering, E., Chang, B.Y., Buggy, J.J., Pals, S.T., and Spaargaren, M. (2012). The clinically active BTK inhibitor PCI-32765 targets B-cell receptor- and chemokine-controlled adhesion and migration in chronic lymphocytic leukemia. Blood *119*, 2590–2594.
3. Herman, S.E.M., Gordon, A.L., Hertlein, E., Ramanunni, A., Zhang, X., Jaglowski, S., Flynn, J., Jones, J., Blum, K.A., Buggy, J.J., et al. (2011). Bruton tyrosine kinase represents a promising therapeutic target for treatment of chronic lymphocytic leukemia and is effectively targeted by PCI-32765. Blood *117*, 6287–6296.
4. Burger, J.A., Tedeschi, A., Barr, P.M., Robak, T., Owen, C., Ghia, P., Bairey, O., Hillmen, P., Bartlett, N.L., Li, J., et al. (2015). Ibrutinib as Initial Therapy for Patients with Chronic Lymphocytic Leukemia. N. Engl. J. Med. *373*, 2425–2437.
5. Messmer, B.T., Messmer, D., Allen, S.L., Kolitz, J.E., Kudalkar, P., Cesar, D., Murphy, E.J., Koduru, P., Ferrarini, M., Zupo, S., et al. (2005). In vivo measurements document the dynamic cellular kinetics of chronic lymphocytic leukemia B cells. J. Clin. Invest. *115*, 755–764.
6. Wodarz, D., Garg, N., Komarova, N.L., Benjamini, O., Keating, M.J., Wierda, W.G., Kantarjian, H., James, D., O'Brien, S., and Burger, J.A. (2014). Kinetics of CLL cells in tissues and blood during therapy with the BTK inhibitor ibrutinib. Blood *123*, 4132–4135.
7. Burger, J.A., Li, K.W., Keating, M.J., Sivina, M., Amer, A.M., Garg, N., Ferrajoli, A., Huang, X., Kantarjian, H., Wierda, W.G., et al. (2017). Leukemia cell proliferation and death in chronic lymphocytic leukemia patients on therapy with the BTK inhibitor ibrutinib. JCI Insight *2*, e89904.
8. Nadler, S.B., Hidalgo, J.H., and Bloch, T. (1962). Prediction of blood volume in normal human adults. Surgery *51*, 224–232.
9. Mayerhoefer, M.E., Haug, A., Jaeger, U., Kazianka, L., Pichler, V., Pfaff, S., Wester, H.J., Hacker, M., and Staber, P.B. (2019). In Human Visualization of Ibrutinib-Induced CLL Compartment Shift. Blood Suppl. *134*, 1750.

10. Herman, S.E.M., Niemann, C.U., Farooqui, M., Jones, J., Mustafa, R.Z., Lipsky, A., Saba, N., Martyr, S., Soto, S., Valdez, J., et al. (2014). Ibrutinib-induced lymphocytosis in patients with chronic lymphocytic leukemia: correlative analyses from a phase II study. Leukemia *28*, 2188–2196.
11. Lewis, S.M., Williams, A., and Eisenbarth, S.C. (2019). Structure and function of the immune system in the spleen. Sci. Immunol. *4*, eaau6085.
12. Chen, J., Moore, A., and Ringshausen, I. (2020). ZAP-70 Shapes the Immune Microenvironment in B Cell Malignancies. Front. Oncol. *10*, 595832.
13. Stapor, P., Weindl, D., Ballnus, B., Hug, S., Loos, C., Fiedler, A., Krause, S., Hroß, S., Fröhlich, F., and Hasenauer, J. (2018). PESTO: Parameter EStimation TOolbox. Bioinformatics *34*, 705–707.
14. Fröhlich, F., Weindl, D., Schälte, Y., Pathirana, D., Paszkowski, Ł., Lines, G.T., Stapor, P., and Hasenauer, J. (2021). AMICI: high-performance sensitivity analysis for large ordinary differential equation models. Bioinformatics *37*, 3676–3677.
15. Loos, C., Krause, S., and Hasenauer, J. (2018). Hierarchical optimization for the efficient parametrization of ODE models. Bioinformatics *34*, 4266–4273.
16. Hass, H., Loos, C., Raimúndez-Álvarez, E., Timmer, J., Hasenauer, J., and Kreutz, C. (2019). Benchmark problems for dynamic modeling of intracellular processes. Bioinformatics *17*, 3073–3082.
17. Schw, G., Heun, L., and Franz, D. (1978). Estimating the Dimension of a Model. Ann. Stat. *2*, 461–464.

STAR★METHODS

KEY RESOURCES TABLE

REAGENT or RESOURCE	SOURCE	IDENTIFIER
Deposited data		
Characteristics and repetitive assessments of lymphocyte counts of 30 CLL patients treated with ibrutinib	Collected in: Jan Burger, Kelvin Li, Mariela Sivina, Ahmed M Amer, Naveen Garg, Alessandra Ferrajoli, Xuelin Huang, Hagop Kantarjian, Susan O'Brien, Marc Hellerstein, Claire Emson, Shih-Shih Chen, Joy Yan, Dominik Wodarz, and Nicholas Chiorazzi. Leukemia cell proliferation and death in chronic lymphocytic leukemia patients on therapy with the btk inhibitor Ibrutinib. JCI Insight, 2, 01 2017 Published: this paper	Shared upon request
Software and algorithms		
MATLAB R2017 b	Mathworks	http://mathworks.com/
PESTO	Stapor et al.[13]	https://github.com/ICB-DCM/PESTO
AMICI	Fröhlich et al.[14]	https://github.com/AMICI-dev/AMICI
code - model simulation, optimization and analysis	this paper	https://doi.org/10.5281/zenodo.11093103

METHOD DETAILS

Clinical data

The dataset used in the study comprises information on 29 patients being treated with ibrutinib while suffering from CLL. It has been collected and used in context of a previous study.[7] Together with basic characteristics such as gender, weight and information on disease specification and progression, 12 to 32 measurements of lymphocyte counts per microliter blood and 2 to 3 volumetric estimations obtained from CT scans of lymph tissue have been collected over a time course of up to 14 months. See Figure 1A for an overview of the clinical data.

Data preprocessing

Several preprocessing steps were executed in previous studies to estimate the total lymphocyte count in peripheral blood, lymph nodes and spleen from relative numbers (counts per μl blood) and tissue volumes.[6,7] To be able to compare our models to the model introduced before, we followed the approach described in the corresponding publication.[6]

Peripheral blood

For each patient and time point, the amount of lymphocytes within peripheral blood was estimated by multiplying the measured number of lymphocytes per microliter with the estimated blood volume of the respective patient. The blood volume was assumed to be constant over time and estimated via the Nadler formula[8] based on gender, height and weight as measured before therapy start:

$$\begin{cases} v_{\mathrm{pb},l} = 0.356 h_m^3 + 0.033 w_{kg} + 0.183 \ \text{ for females} \\ v_{\mathrm{pb},l} = 0.367 h_m^3 + 0.032 w_{kg} + 0.604 \ \text{ for males.} \end{cases}$$

Here, $v_{\mathrm{pb},l}$, h_m and w_{kg} denote the blood volume in liters, height in meters and weight in kilograms, respectively.

Spleen and lymph nodes

First, tissue volume was estimated from CT scans of lymph nodes and spleen. We refer to Burger et al.[7] for details on the procedure. Our calculations are based on the provided volume estimations.

Second, we estimated lymphocyte counts from tissue volumes. Whereas the 2-compartment models have been fitted to data comprising both spleen and lymph nodes (see Wodarz et al.[6]), the 3-compartment models are based on data treating both tissues separately. As such, the preprocessing steps differ.

2-compartment models

In Wodarz et al.,[6] it is assumed that the volume drop of the lymph nodes represented the decline of cancerous tissue more appropriate than the regression of spleen volume. As such, the authors adapted the volume estimations of the latter organ to display the same decline as the lymph nodes by inferring and applying an exponential decline rate. We refer to the sum of the volume of all lymph tissue sites as *raw lymph tissue volume*, and to the sum obtained after adapting the spleen volume to the *adapted lymph tissue volume*. The number of cells in the lymph tissue was calculated from the adapted lymph tissue volume and the average volume of a B-lymphocyte of 166 fL (*fL*). An overview of the approach is visualized in Figure S1.

Precisely, the following calculations have been performed: For every patient, the total volume of the lymph tissue, v_{lt}, at time point $t_1 = 0$, was obtained by adding the respective estimated volumes of spleen, intra-abdominal, inguinal and axillary lymph nodes:

$$v_{\mathrm{lt}}(t_1) = \sum_{j=1}^{N_{\mathrm{ln}}} v_{\mathrm{ln}_j}(t_1) + v_{\mathrm{sp}}(t_1).$$

Here, N_{ln} denotes the number of scanned lymph nodes. For subsequent samples, Wodarz et al. assumed that the measured drop in spleen volume did not represent the effective decrease in lymphocyte counts within that tissue.[6] Thus, the volume decline of the lymph tissue was inferred from the decline of the lymph nodes as follows: With N_{ln} and $v_{\mathrm{ln}_j}(t_i)$ denoting the number of scanned lymph nodes and the estimated volume of lymph node j at time point i, respectively, the average decline rate of the lymph nodes was computed as

$$r_i = \frac{1}{N_{\mathrm{ln}}} \sum_{j=1}^{N_{\mathrm{ln}}} \frac{1}{t_i - t_{i-1}} \ln \frac{v_{\mathrm{ln}_j}(t_{i-1})}{v_{\mathrm{ln}_j}(t_i)}. \qquad \text{(Equation 1)}$$

Here, the summand represents the rate of volume decline of lymph node j between the observed time points, assuming constant exponential decay. With $v_{\mathrm{sp}}(t_i)$ and $v_{\mathrm{lt}}(t_i)$ referencing the volume of spleen and total lymph tissue at timepoint t_i, respectively, the lymph tissue volume was recursively estimated as

$$\begin{aligned} v_{\mathrm{lt}}(t_1) &= \sum_{j=1}^{N_{\mathrm{ln}}} v_{\mathrm{ln}_j}(t_1) + v_{\mathrm{sp}}(t_1) \\ v_{\mathrm{lt}}(t_i) &= v_{\mathrm{lt}}(t_{i-1}) \exp(-r_i(t_i - t_{i-1})), i > 1, \end{aligned} \qquad \text{(Equation 2)}$$

such that the decline of the combined lymph tissue corresponds to the average decline of the lymph nodes.

Finally, the total number of lymphocytes used for fitting was obtained by dividing the estimated volume by the average volume of a CLL cell, namely 166fL, as used in Wodarz et al.[6]:

$$n_{\mathrm{lt,observed}}(t) = \frac{v_{\mathrm{lt}}(t)}{166} 10^{12}.$$

3-compartment models

As before, the volume of the lymph nodes was obtained by summing up the estimated volumes of the scanned intra-abdominal, inguinal and axillary lymph nodes. For both lymph tissue compartments, the total numbers of lymphocytes used for fitting were assessed from the volume estimations by dividing through the average volume of a CLL cell:

$$\begin{aligned} n_{\mathrm{ln,observed}}(t) &= \frac{\sum_{j=1}^{N_{\mathrm{ln}}} v_{\mathrm{ln}_j}(t)}{166} 10^{12} \\ n_{\mathrm{sp,observed}}(t) &= \frac{v_{\mathrm{sp}}(t)}{166} 10^{12}. \end{aligned}$$

Remark 1. The first measurement of the lymph tissue has been taken several weeks before treatment started. We resetted the measurement time to day zero and accounted for the variability within the parameter estimation process, estimating the initial cancer burden as an optimization parameter. The applied time shift ranges from 103 to 62 days.

Remark 2. From now on, we refer to the number of cells estimated from the data as measurement data. To compare our models to the reference model, we adopted the approach of data preprocessing and the objective function for parameter optimization described in the corresponding publication.[6]

Model design

To discriminate between the considered models, we classified them as *homogeneous* and *heterogeneous compartment* models. The discrimination was applied to both the 2- and 3-compartment models.

Homogeneous compartment model family

If we assume that all lymphocytes within a compartment react to ibrutinib homogeneously, the considered processes such as cell death and redistribution would act on the whole population of lymphocytes within the respective site. As proliferation is expected to be inhibited due to the treatment, that would result in a model with all cells leaving the system over time. As this phenomenon is not visible in the data, it was suggested to add a constant influx into the lymph tissue compartment to enable a stabilization of the solution above zero.[6] Models following this hypothesis are referred to as *homogeneous compartment* models. Precisely, if $n_{\text{unstable}}(t)$ denotes the number of lymphocytes without influx, the stabilization is obtained by modifying the kinetic equation as follows:

$$\frac{d}{dt}n_{\text{stable}}(t) = \frac{d}{dt}n_{\text{unstable}}(t) + c. \qquad \text{(Equation 3)}$$

Remark. In Wodarz et al.,[6] the influx is equivalently parameterised as dc. Precisely, the equations read as

$$\frac{d}{dt}n^{wod}_{\text{stable}}(t) = \frac{d}{dt}n^{wod}_{\text{unstable}}(t) + dc, \qquad \text{(Equation 4)}$$

and solutions to 4 can be obtained from solutions to 3 by substituting parameter c with $\frac{c}{d}$.

Heterogeneous compartment model family

Alternatively, we can consider the observed cell compartments as as heterogeneous entity comprising cells responding and not responding to ibrutinib. In the lymph tissue, the non-responding sub population might represent normal tissue not consisting of lymphocytes, whereas in the peripheral blood, we describe a healthy level of lymphocytes the blood system is trying to reestablish in the long term. Models allowing for non responding sub populations are referred to as *heterogeneous compartment* models. With $n_{\text{observed}}(t)$ and n_{constant} denoting the measured number of lymphocytes and the size of the unaffected sub population, respectively, the kinetics read as follows:

$$\begin{aligned}\frac{d}{dt}n_{\text{observed}}(t) &= \frac{d}{dt}(n_{\text{observed}}(t) - n_{\text{constant}}) + \frac{d}{dt}n_{\text{constant}} \\ &= \frac{d}{dt}(n_{\text{observed}}(t) - n_{\text{constant}}).\end{aligned} \qquad \text{(Equation 5)}$$

Here, the kinetic describing $n_{\text{observed}}(t) - n_{\text{constant}}$ matches the kinetic of the unstable solution as introduced above.

Differential equations

In the following, we derive the equations and solutions of the maximal models of the homogeneous 2-compartment and the heterogeneous 2- and 3-compartment models, e.g., the models where all considered processes are apparent. The reduced models can be obtained by setting the corresponding rates to 0.

Homogeneous 2-compartment model

Let $n_{\text{lt}}(t), n_{\text{pb}}(t)$ be the total number of lymphocytes in lymph tissue and peripheral blood compartment, respectively. The maximal model of the model class is defined by the following processes:

1 Cell death in both compartments, parameterized with $d_{\text{lt}}, d_{\text{p}}$.
2 Redistribution from lymph tissue to peripheral blood compartment, parameterized with $m_{\text{lt}\to\text{lt}\to\text{p}}$.
3 Constant influx into the lymph tissue, parameterized with $c_{\text{lt}}, c_{\text{pb}}$.

All rates are assumed to be constant over time. As such, the ordinary differential equations are given as

$$\begin{cases}\frac{d}{dt}n_{\text{lt}}(t) = -\left(d_{\text{lt}} + m_{\text{lt}\to\text{pb}}\right)n_{\text{lt}}(t) + c_{\text{lt}} \\ \frac{d}{dt}n_{\text{pb}}(t) = -d_{\text{pb}}n_{\text{pb}}(t) + m_{\text{lt}\to\text{pb}}n_{\text{lt}}(t) + c_{\text{pb}},\end{cases} \qquad \text{(Equation 6)}$$

with initial conditions $n_{\text{lt}}(0) = LT_0$ and $n_{\text{pb}}(0) = PB_0$, both parameters to be estimated. Using variation of the constants, we compute the analytical solutions. With $\alpha_{\text{lt}\to} := d_{\text{lt}} + m_{\text{lt}\to\text{pb}}$, we abbreviate the parameter quantifying the outflux of the lymph tissue compartment. As such, the solution to the lymph tissue compartment reads as

$$\begin{aligned} n_{\mathrm{lt}}(t) &= \frac{c_{\mathrm{lt}}}{\alpha_{\mathrm{lt}\rightarrow}} + \left(LT_0 - \frac{c_{\mathrm{lt}}}{\alpha_{\mathrm{lt}\rightarrow}}\right)\exp^{-\alpha_{\mathrm{lt}\rightarrow}t} \\ &= B_{\mathrm{lt}_c} + B_{\mathrm{lt}_{\alpha_{\mathrm{lt}\rightarrow}}}\exp^{-\alpha_{\mathrm{lt}\rightarrow}t}. \end{aligned} \quad \text{(Equation 7)}$$

For brevity, we write $B_{\mathrm{lt}_c} := \frac{c_{\mathrm{lt}}}{\alpha_{\mathrm{lt}\rightarrow}}$ and $B_{\mathrm{lt}_{\alpha_{\mathrm{lt}\rightarrow}}} := LT_0 - B_{\mathrm{lt}_c}$ as the coefficients of the constant and the exponential term, respectively.

With $\alpha_{\mathrm{pb}\rightarrow} := d_{\mathrm{pb}}$ the parameter quantifying outflux from peripheral blood, and $B_{\mathrm{pb}_c}, B_{\mathrm{pb}_{\alpha_{\mathrm{lt}\rightarrow}}}, B_{\mathrm{pb}_{\alpha_{\mathrm{pb}\rightarrow}}}$ denoting the coefficients of constant and corresponding exponential terms, the solution to the peripheral blood reads as

$$\begin{aligned} n_{\mathrm{pb}}(t) &= \frac{m_{\mathrm{lt}\rightarrow\mathrm{pb}}B_{\mathrm{lt}_c}+c_{\mathrm{pb}}}{\alpha_{\mathrm{pb}\rightarrow}} + \\ &\quad \frac{m_{\mathrm{lt}\rightarrow\mathrm{pb}}B_{\mathrm{lt}_{\alpha_{\mathrm{lt}\rightarrow}}}}{\alpha_{\mathrm{pb}\rightarrow} - \alpha_{\mathrm{lt}\rightarrow}}\exp^{-\alpha_{\mathrm{lt}\rightarrow}t} + \\ &\quad \left(PB_0 - \frac{m_{\mathrm{lt}\rightarrow\mathrm{pb}}B_{\mathrm{lt}_c}+c_{\mathrm{pb}}}{\alpha_{\mathrm{pb}\rightarrow}} - \frac{m_{\mathrm{lt}\rightarrow\mathrm{pb}}B_{\mathrm{lt}_{\alpha_{\mathrm{lt}\rightarrow}}}}{\alpha_{\mathrm{pb}\rightarrow} - \alpha_{\mathrm{lt}\rightarrow}}\right)\exp^{-\alpha_{\mathrm{pb}\rightarrow}t} \\ &= B_{\mathrm{pb}_c} + B_{\mathrm{pb}_{\alpha_{\mathrm{lt}\rightarrow}}}\exp^{-\alpha_{\mathrm{lt}\rightarrow}t} + \left(PB_0 - B_{\mathrm{pb}_c} - B_{\mathrm{pb}_{\alpha_{\mathrm{lt}\rightarrow}}}\right)\exp^{-\alpha_{\mathrm{pb}\rightarrow}t} \\ &= B_{\mathrm{pb}_c} + B_{\mathrm{pb}_{\alpha_{\mathrm{lt}\rightarrow}}}\exp^{-\alpha_{\mathrm{lt}\rightarrow}t} + B_{\mathrm{pb}_{\alpha_{\mathrm{pb}\rightarrow}}}\exp^{-\alpha_{\mathrm{pb}\rightarrow}t}. \end{aligned} \quad \text{(Equation 8)}$$

Together, Equations 7 and 8 provide a solution to system 6:

$$\begin{cases} n_{\mathrm{lt}}(t) = B_{\mathrm{lt}_c} + B_{\mathrm{lt}_{\alpha_{\mathrm{lt}\rightarrow}}}\exp^{-\alpha_{\mathrm{lt}\rightarrow}t} \\ n_{\mathrm{pb}}(t) = B_{\mathrm{pb}_c} + B_{\mathrm{pb}_{\alpha_{\mathrm{lt}\rightarrow}}}\exp^{-\alpha_{\mathrm{lt}\rightarrow}t} + B_{\mathrm{pb}_{\alpha_{\mathrm{pb}\rightarrow}}}\exp^{-\alpha_{\mathrm{pb}\rightarrow}t}. \end{cases} \quad \text{(Equation 9)}$$

Remark 1. Cell death and constant influxes can but must not be apparent in the lymph tissue and peripheral blood compartments, respectively. After visually expecting the data, we do not consider redistribution from the peripheral blood to the lymph tissue, while redistribution from lymph tissue to peripheral blood can be existent or not. This makes it a total of

$$2^{2\cdot 2}\cdot 2 = 32 \quad \text{(Equation 10)}$$

models within the homogeneous 2-compartment model class.

Remark 2. The reference model introduced in Wodarz et al.Wodarz.14 belongs to the family of homogeneous 2-compartment models and is fitted and analyzed within the optimization of that model class. Precisely, it is defined by the following processes.

1 Cell death in both compartments, parameterized with b $d_{\mathrm{lt}}, d_{\mathrm{p}}$.
2 Redistribution from lymph tissue to peripheral blood compartment, parameterized with b $m_{\mathrm{lt}\rightarrow\mathrm{p}}$.
3 Constant influx into the lymph tissue, parameterized with c_{lt}.

Thus, equations and solutions to the reference model are obtained by setting $c_{\mathrm{pb}} := 0$ in 6 and 9.

Heterogeneous 2-compartment model

In the heterogeneous models, the cell populations are split into dynamical and constant subpopulations. Therefore, we derive the equations of the dynamical solutions, the total number of cells is then obtained by adding the size of the constant subcompartment, as sketched in Equation 5. Let $\tilde{n}_{\mathrm{lt}}(t), \tilde{n}_{\mathrm{pb}}(t)$ be the total number of lymphocytes in non constant lymph tissue and peripheral blood compartment, respectively. Again, we derive equations and solutions for the model with cells trafficking from lymph tissue to peripheral blood, the model with cells redistributing into the other direction is constructed accordingly. Similar to the homogeneous compartment model, the model defining the kinetics of the dynamical subpopulation is defined by the following processes:

1 Cell death in both compartments, parameterized with $d_{\mathrm{lt}}, d_{\mathrm{pb}}$.
2 Redistribution from lymph tissue to peripheral blood compartment, parameterized with $m_{\mathrm{lt}\rightarrow\mathrm{pb}}$.

No influx is necessary, as the stabilization is achieved with the constant subpopulations. As such, the ordinary differential equations are given as

$$\begin{cases} \frac{d}{dt}\tilde{n}_{\mathrm{lt}}(t) = -\left(d_{\mathrm{lt}} + m_{\mathrm{lt}\rightarrow\mathrm{pb}}\right)\tilde{n}_{\mathrm{lt}}(t) \\ \frac{d}{dt}\tilde{n}_{\mathrm{pb}}(t) = -d_{\mathrm{pb}}\tilde{n}_{\mathrm{pb}}(t) + m_{\mathrm{lt}\rightarrow\mathrm{pb}}\tilde{n}_{\mathrm{lt}}(t), \end{cases} \quad \text{(Equation 11)}$$

with initial conditions $\tilde{n}_{\mathrm{lt}}(0) = LT_0 - LT_c$ and $\tilde{n}_{\mathrm{pb}}(0) = PB_0 - PB_c$, with LT_c and PB_c the size of the constant subcompartments, and all parameters to be estimated from the data. As before, the analytical solutions can be computed applying variation of the constants. With the same notation as before, one obtains

$$\begin{aligned}\tilde{n}_{\mathrm{lt}}(t) &= (LT_0 - LT_c)\exp^{-\alpha_{\mathrm{lt}\to}t} \\ &= B_{\mathrm{lt}_{\alpha_{\mathrm{lt}\to}}}\exp^{-\alpha_{\mathrm{lt}\to}t},\end{aligned} \tag{Equation 12}$$

$B_{\mathrm{lt}_{\alpha_{\mathrm{lt}\to}}} := LT_0 - LT_c$ denoting the coefficient of the exponential term.
For the peripheral blood, we obtain

$$\begin{aligned}\tilde{n}_{\mathrm{pb}}(t) &= \frac{m_{\mathrm{lt}\to\mathrm{pb}}B_{\mathrm{lt}_{\alpha_{\mathrm{lt}\to}}}}{\alpha_{\mathrm{pb}\to} - \alpha_{\mathrm{lt}\to}}\exp^{-\alpha_{\mathrm{lt}\to}t} + \\ &\quad \left(PB_0 - PB_c - \frac{m_{\mathrm{lt}\to\mathrm{pb}}B_{\mathrm{lt}_{\alpha_{\mathrm{lt}\to}}}}{\alpha_{\mathrm{pb}\to} - \alpha_{\mathrm{lt}\to}}\right)\exp^{-\alpha_{\mathrm{pb}\to}t} \\ &= B_{\mathrm{pb}_{\alpha_{\mathrm{lt}\to}}}\exp^{-\alpha_{\mathrm{lt}\to}t} + \left(PB_0 - PB_c - B_{\mathrm{pb}_{\alpha_{\mathrm{lt}\to}}}\right)\exp^{-\alpha_{\mathrm{pb}\to}t} \\ &= B_{\mathrm{pb}_{\alpha_{\mathrm{lt}\to}}}\exp^{-\alpha_{\mathrm{lt}\to}t} + B_{\mathrm{pb}_{\alpha_{\mathrm{pb}\to}}}\exp^{-\alpha_{\mathrm{pb}\to}t}.\end{aligned} \tag{Equation 13}$$

With that, the solutions to the heterogeneous 2-compartment model 11 are given as

$$\begin{cases} n_{\mathrm{lt}}(t) = B_{\mathrm{lt}_{\alpha_{\mathrm{lt}\to}}}\exp^{-\alpha_{\mathrm{lt}\to}t} + LT_c \\ n_{\mathrm{pb}}(t) = B_{\mathrm{pb}_{\alpha_{\mathrm{lt}\to}}}\exp^{-\alpha_{\mathrm{lt}\to}t} + B_{\mathrm{pb}_{\alpha_{\mathrm{pb}\to}}}\exp^{-\alpha_{\mathrm{pb}\to}t} + PB_c. \end{cases} \tag{Equation 14}$$

Remark. As in the family of homogeneous 2-compartment models, cell death and constant subpopulations can but must not be apparent in the lymph tissue and peripheral blood compartments. We consider redistribution being non-existent or going from lymph tissue to peripheral blood, leading to a total of

$$2^{2\cdot 2}\cdot 2 = 32 \tag{Equation 15}$$

models within that model class.

Homogeneous 3-compartment model

As the homogeneous 2-compartment models were outperformed by heterogeneous 2-compartment models in the first step of our analysis, we did not consider the homogeneous model family when selecting 3-compartment models.

Heterogeneous 3-compartment model

In the following, we derive equations and solutions to the maximal heterogeneous 3-compartment model where cells redistribute from spleen to lymph nodes and peripheral blood and from lymph nodes to peripheral blood. Submodels are obtained by setting rates to 0, models with different redistribution reactions by interchanging the corresponding observables. Again, we start deriving the equations for the subcompartments consisting of cells affected by ibrutinib. The kinetics are defined through the following processes.

1 Cell death in all compartments, parameterized with $d_{\mathrm{sp}}, d_{\mathrm{ln}}, d_{\mathrm{pb}}$.
2 Redistributions from spleen to lymph node and peripheral blood and from lymph node to peripheral blood compartments, parameterized with $m_{\mathrm{sp}\to\mathrm{ln}}$, $m_{\mathrm{sp}\to\mathrm{pb}}$, $m_{\mathrm{ln}\to\mathrm{pb}}$.

This translates into the following 3-dimensional system of ordinary differential equations:

$$\begin{cases} \frac{d}{dt}\tilde{n}_{\mathrm{sp}}(t) = -\left(d_{\mathrm{sp}} + m_{\mathrm{sp}\to\mathrm{pb}} + m_{\mathrm{sp}\to\mathrm{ln}}\right)\tilde{n}_{\mathrm{sp}}(t) \\ \frac{d}{dt}\tilde{n}_{\mathrm{ln}}(t) = -\left(d_{\mathrm{ln}} + m_{\mathrm{ln}\to\mathrm{pb}}\right)\tilde{n}_{\mathrm{ln}}(t) + m_{\mathrm{sp}\to\mathrm{ln}}\tilde{n}_{\mathrm{sp}}(t) \\ \frac{d}{dt}\tilde{n}_{\mathrm{pb}}(t) = -d_{\mathrm{pb}}\tilde{n}_{\mathrm{pb}}(t) + m_{\mathrm{sp}\to\mathrm{pb}}\tilde{n}_{\mathrm{sp}}(t) + m_{\mathrm{ln}\to\mathrm{pb}}\tilde{n}_{\mathrm{ln}}(t). \end{cases} \tag{Equation 16}$$

We use analogous abbreviations as before and write $\alpha_{\mathrm{sp}\to} := d_{\mathrm{sp}} + m_{\mathrm{sp}\to\mathrm{pb}} + m_{\mathrm{sp}\to\mathrm{ln}}$ and $\alpha_{\mathrm{ln}\to} := d_{\mathrm{ln}} + m_{\mathrm{ln}\to\mathrm{pb}}$ to quantify the outflux from the spleen and lymph node compartment, respectively. The solutions to those two tissues read exactly as the solutions of the 2-compartment model, the spleen now representing the compartment with only outflux, as the lymph tissue before, the lymph nodes representing the compartment with influx from one compartment and an outflux, as the peripheral blood before. As such, the solutions are given as

$$\begin{aligned}\tilde{n}_{sp}(t) &= (SP_0 - SP_c)\exp^{-\alpha_{sp\to t}} \\ &= B_{sp_{\alpha_{sp\to}}}\exp^{-\alpha_{sp\to t}}\end{aligned} \quad \text{(Equation 17)}$$

and

$$\begin{aligned}\tilde{n}_{ln}(t) &= \frac{m_{sp\to ln}B_{sp_{\alpha_{sp\to}}}}{\alpha_{ln\to} - \alpha_{sp\to}}\exp^{-\alpha_{sp\to t}} + \\ &\quad \left(LN_0 - LN_c - \frac{m_{sp\to ln}B_{sp_{\alpha_{sp\to}}}}{\alpha_{ln\to} - \alpha_{sp\to}}\right)\exp^{-\alpha_{ln\to t}} \\ &= B_{ln_{\alpha_{sp\to}}}\exp^{-\alpha_{sp\to}t} + \left(LN_0 - LN_c - B_{ln_{\alpha_{sp\to}}}\right)\exp^{-\alpha_{ln\to t}} \\ &= B_{ln_{\alpha_{sp\to}}}\exp^{-\alpha_{sp\to t}} + B_{ln_{\alpha_{ln\to}}}\exp^{-\alpha_{ln\to t}}.\end{aligned} \quad \text{(Equation 18)}$$

For the third, the peripheral blood compartment, we have to compute the solution to the dynamical subcompartment comprising influx from both the other compartments and an outflux. We can apply variation of the constants to obtain the solution:

$$\begin{aligned}\tilde{n}_{pb}(t) &= \frac{m_{ln\to pb}+m_{sp\to pb}}{\alpha_{pb\to} - \alpha_{sp\to}}B_{ln_{\alpha_{sp\to}}}\exp^{-\alpha_{sp\to t}} + \\ &\quad \frac{m_{ln\to pb}}{\alpha_{pb\to} - \alpha_{ln\to}}B_{ln_{\alpha_{ln\to}}}\exp^{-\alpha_{ln\to t}} + \\ &\quad \left(PB_0 - PB_c - \frac{m_{ln\to pb}+m_{sp\to pb}}{\alpha_{pb\to} - \alpha_{sp\to}}B_{ln_{\alpha_{sp\to}}} - \frac{m_{ln\to pb}}{\alpha_{pb\to} - \alpha_{ln\to}}B_{ln_{\alpha_{ln\to}}}\right)\exp^{-\alpha_{pb\to t}} \\ &= B_{pb_{\alpha_{sp\to}}}\exp^{-\alpha_{sp\to t}} + B_{pb_{\alpha_{ln\to}}}\exp^{-\alpha_{ln\to t}} + \\ &\quad \left(PB_0 - PB_c - B_{pb_{\alpha_{sp\to}}} - B_{pb_{\alpha_{ln\to}}}\right)\exp^{-\alpha_{pb\to t}} \\ &= B_{pb_{\alpha_{sp\to}}}\exp^{-\alpha_{sp\to t}} + B_{pb_{\alpha_{ln\to}}}\exp^{-\alpha_{ln\to t}} + B_{pb_{\alpha_{pb\to}}}\exp^{-\alpha_{pb\to t}}.\end{aligned} \quad \text{(Equation 19)}$$

Combining Equations 17, 18, and 19, the solutions to 16 read as

$$\begin{cases} n_{sp}(t) = B_{sp_{\alpha_{sp\to}}}\exp^{-\alpha_{sp\to t}} + SP_c \\ n_{ln}(t) = B_{ln_{\alpha_{sp\to}}}\exp^{-\alpha_{sp\to t}} + B_{ln_{\alpha_{ln\to}}}\exp^{-\alpha_{ln\to t}} + LN_c \\ n_{pb}(t) = B_{pb_{\alpha_{sp\to}}}\exp^{-\alpha_{sp\to t}} + B_{pb_{\alpha_{ln\to}}}\exp^{-\alpha_{ln\to t}} + B_{pb_{\alpha_{pb\to}}}\exp^{-\alpha_{pb\to t}} + PB_c. \end{cases} \quad \text{(Equation 20)}$$

Remark. Again, cell death and constant subpopulations can but must not be apparent in the three compartments representing lymph nodes, spleen and peripheral blood. Redistribution between each combination of two distinct compartments can be non-existent or be apparent in one of two directions. We do not consider redistributions in both directions at a time. This makes it a total of

$$2^{2\cdot 3}\cdot 3^3 = 1728 \quad \text{(Equation 21)}$$

models within the class of heterogeneous 3-compartment models.

Parameter optimization

Noise model

Building on a previous study, we did not optimize the loss between the total number of cells measured and estimated by the solution to the ODE system directly but scaled both by a factor depending on the respective compartment.[6] With that, we accounted for the varying amount of measurements and compartment sizes that might lead to overfitting one tissue site. To account for measurement noise and errors within data preprocessing and the model, we assumed constant additive Gaussian noise on the scaled measurements with mean 0 and standard deviation σ estimated as additional parameter for every patient. Here, we assumed that both measurement noise and model error are constant over time and jointly contribute to the observed variability. Additionally, we assumed the same noise on all compartments scaled by compartment size.

Derivation of the loss function

Based on the considerations and assumptions described in the previous section, we derive the objective function used in our parameter estimation.

Let $n_{meas,c} = (n_{meas,c,t_1}, \ldots n_{meas,c,t_{N_c}})$ be the measurement data in compartment c taken on N_c time points, and $\|n_{meas,c}\|_2 = \sqrt{\sum_{i=1}^{N_c} n_{meas,c,t_i}^2}$ the corresponding l2-Norm. If $n_{sol,c}(\theta)$, the analytical solution of the model depending on parameter vector θ, is an estimation of the measurement data, $\frac{n_{sol,c}(\theta)}{\|n_{meas,c}\|_2}$ is an estimation for $\frac{n_{meas,c}}{\|n_{meas,c}\|_2}$. Corresponding to the least-square optimization used in Wodarz et al.,[6] we assumed additive Gaussian noise on the scaled measurements with mean 0 and standard deviation σ. With that, the likelihood for one scaled data point reads as follows:

$$p\left(\frac{n_{meas,c,t_i}}{\|n_{meas,c}\|_2}|(\theta,\sigma)\right) = \frac{1}{\sqrt{2\pi}\sigma}\exp\left(-\frac{(n_{meas,c,t_i} - n_{sol,c}(\theta,t_i))^2}{2\|n_{meas,c}\|_2\sigma^2}\right).$$

Note that we optimized only one parameter for the standard deviation for all compartments. With $\mathcal{D}$ denoting all measurements within the dataset, scaled as explained before, we aimed at maximizing the joint likelihood function explaining $\mathcal{D}$. For numerical reasons, we chose to minimize the negative log likelihood instead of maximizing the likelihood, resulting in the following objective function:

$$\begin{aligned}
&-\log(P(\mathcal{D}|\theta,\sigma)) \\
&= -\log\left(\prod_{c\text{ in }C}\prod_{i=1}^{N_c}\frac{1}{\sqrt{2\pi}\sigma}\exp\left(-\frac{(n_{meas,c,t_i} - n_{sol,c}(\theta,t_i))^2}{2\|n_{meas,c}\|_2\sigma^2}\right)\right) \\
&= -\sum_{c\text{ in }C}\sum_{i=1}^{N_c}\log\left(\frac{1}{\sqrt{2\pi}\sigma}\exp\left(-\frac{(n_{meas,c,t_i} - n_{sol,c}(\theta,t_i))^2}{2\|n_{meas,c}\|_2\sigma^2}\right)\right) \\
&= \frac{1}{2}\sum_{c\text{ in }C}\sum_{i=1}^{N_c}\left(\log(2\pi\sigma^2) + \left(\frac{n_{meas,c,t_i} - n_{sol,c}(\theta,t_i)}{\|n_{meas,c}\|_2\sigma}\right)^2\right) \\
&= \sum_{c\text{ in }C}\frac{N_c}{2}\log(2\pi\sigma^2) + \frac{1}{2\sigma^2}\sum_{c\text{ in }C}\sum_{i=1}^{N_c}\left(\frac{n_{meas,c,t_i} - n_{sol,c}(\theta,t_i)}{\|n_{meas,c}\|_2}\right)^2.
\end{aligned} \quad \text{(Equation 22)}$$

with C the set of compartments considered in the respective used model.

Remark. We chose to add the standard deviation as an additional parameter as we aimed for a likelihood based approach for model comparison. If we would have fixed σ and only optimized the parameters of the kinetic model, 22 simplified to the objective function used in Wodarz et al.[6]

Optimization procedure

For all models considered, we estimated the kinetic rates corresponding to death and migration processes as well as the initial number of cells within the respective compartments. This allows for flexibility of the solution also at the first time point that might arise due to measurement noise, perturbation introduced within the estimation of absolute cells from relative or volumetric data or the fact that the first measurement has not been taken exactly on the first day of treatment for all patients. For all models and patients we also inferred one noise parameter σ, determining the spread of the Gaussian noise model. To improve the optimization procedure in speed and accuracy, we followed a hierarchical optimization approach as described in Loos et al.[15] We assumed that all parameters are constant over time. Due to their biological nature, the kinetic rates and constants are positive, allowing for optimization in log10 scale.[16] We performed multi-start local optimization of the objective function 22 using the parameter estimation toolbox PESTO.[13]

Parameter identifiability

Analyzing the analytical solutions to the equations of both the homogeneous and the heterogeneous compartment models, it can be shown that all model parameters are theoretically identifiable.

To test practical identifiability of the model parameters, we investigate the likelihood profiles of the best performing models of all model classes. We find identifiability issues in 12 patients for the homogeneous 2-compartment models, in 6 patients for the heterogeneous 2-compartment models and in 10 patients for the 3-compartment models. The issues mainly arise in parameters quantifying cell decline in lymphoid organs, which has also been reported in Burger et al.,[7] where the same data was used to estimate parameters of a specific homogeneous 2-compartment model. Non-identifiable parameters are summarized in Table S1, supplementary materials. As we remove patients with unidentifiable parameters for the quantitative analysis on the estimated parameter values, we do not consider this a major issue. However, tissue data at earlier time points most likely improve parameter estimates, might have an impact on results of the model selection and improve the statistical power of our analysis.

Model selection

Whenever we compared within a set of models, we applied the Bayesian information criterion (BIC)[17] to find the best or to reject a model. It is computed as

$$BIC = \log(|\mathcal{D}|)n_{\text{params}} - 2\log(P(\mathcal{D}|\theta,\sigma)),$$

where $|\mathcal{D}|$ and n_{params} are the number of data points and estimated parameters, respectively. All comparisons were performed at patient-level. The number of parameters varies between models (2–12), while the number of data points varies between patients. The BIC rewards high likelihood values and thus favors models that are able to explain the measurement data. On the other hand, it penalizes the model complexity in the form of additional model parameters that, in our case, correspond to kinetic reactions. The model with minimal BIC was considered as the best, models whose BIC differs from the minimal by less than 2 were considered as equally good. If difference to the minimal BIC was greater than 10, a model was rejected.

Model selection 3-compartment models

When finding the best 3-compartment model for each patient, we took a total of 1728 model architectures into account. We only considered heterogeneous models, as they outperformed the homogeneous models in the case of 2-compartment models. To reduce computational effort, we applied a hierarchical model selection process as follows: All models were grouped based on existence and direction of redistribution processes. For any combination of two distinct compartments *A* and *B*, a connection might not exist, go from *A* to *B*, i.e., that cells distribute from compartment *A* to *B*, or go from *B* to *A*, which made it a total of $3^3 = 27$ subgroups. We disregarded the two circular models, which left 25 model subgroups. While all models within such a subgroup share the redistribution processes between the compartments, they differ in the existence of cell death and constant subpopulations within the three compartments. Thus, each subgroup consists of 2^6 models. For model selection, parameters of the most complex models of each subgroup, e.g., the models with cell death and subpopulations considered in all compartments, were optimized and, based on the Bayesian information criterion, the best performing complex models were selected. Second, the selected complex models were reduced by setting one or more parameters representing cell death and constant subpopulations to 0. Again, the Bayesian information criterion was applied to the resulting set of models to find the best 3-compartment model. The model selection pipeline was applied to every patient individually.

Model selection 2- vs. 3-compartment models

Whereas the 2-compartmental models were fitted to combined lymph tissue data after adaption of the spleen volume, the 3-compartmental model was fitted to lymphocyte counts estimated from spleen and lymph node values separately without further adaptions. To compare model performance quantitatively, the solutions must be projected to predict the same target. We decided to perform the model comparison on the total number of lymphocytes estimated from blood counts and the raw lymph tissue data. With that, we wanted to reduce bias induced by adapting the data. The corresponding fit based on the 3-compartment model was obtained by summing up the solutions for lymph nodes and spleen, respectively. For the 2-compartment models, we reversed the pre-processing of the data by adding the difference of the measured and inferred lymph tissue data to the optimized solution. An overview of the approach is visualized in Figure S2.

Precisely, using the previous notation, $v_{\text{lt}}(t_i)$ denoting the inferred lymph tissue volume at time point t_i as defined in Equation 2 and $n_{\text{sol,lt}}(\theta, t_i)$ a solution predicting $v_{\text{lt}}(t_i)$, we projected the latter as

$$n_{\text{sol,ln+sp}}(\theta, t_i) = n_{\text{sol,lt}}(\theta, t_i) + \left(\sum_{j=1}^{N_{\text{ln}}} v_{\text{ln}_j}(t_i) + v_{\text{sp}}(t_i)\right) 166fL$$

to obtain an estimation of the total lymphocyte count in spleen and lymph nodes. With that we resembled the assumption that the inferred volume accounts for the actual decline that is what the model solution predicts, whereas the remaining volume stays constant and has to be added to the obtained solution.

QUANTIFICATION AND STATISTICAL ANALYSIS

Statistical analysis was performed in MATLAB to analyze model parameters and performance with clinical parameters. Number of datapoints of the respective tests are to be found in Table 1 and section. Tests are assumed to be statistically significant with a *p*-value 0f 0.05. Due to the small dataset, the data can not be assumed to be normally distributed. Hence, statistical tests with few assumptions on the distribution of the data was used. Symmetry of the data distribution was visually examined using histograms automatically binned with the MATLAB function histogram.

During the preparation of this work the author(s) used ChatGPT in order to enhance the manuscript's language. After using this tool/service, the author(s) reviewed and edited the content as needed and take(s) full responsibility for the content of the publication.